JOURNAL OF SOLID STATE CHEMISTRY 66, 7–19 (1987)

The Stability and Structure of $Cs_x[Ti_{2-x/4}\square_{x/4}]O_4$, $0.61 < x < 0.65$

I. E. GREY, C. LI, I. C. MADSEN, AND J. A. WATTS

CSIRO Division of Mineral Chemistry, P.O. Box 124, Port Melbourne, Victoria, Australia

Received December 16, 1985; in revised form April 21, 1986

The stability of the phase $Cs_x[Ti_{2-x/4}\square_{x/4}]O_4$, $\square$ = vacancy, in the Cs_2O–TiO_2 system has been studied in the temperature range 800–1120°C. The phase has a narrow range of homogeneity with $0.61 < x < 0.65$. Structure refinements were carried out for X-ray intensity data from two crystals obtained from melts with $TiO_2 : CsO_{0.5}$ molar ratios of 2.0 and 3.2. The crystals have orthorhombic symmetry, *Immm*, $a_0 = 3.83$, $b_0 = 17.00$, $c_0 = 2.96$ Å. The refinements are consistent with the structural model of Hervieu and Raveau (*Rev. Chim. Minér.* **18**, 642 (1981)) in which (010) corrugated layers of titanium–oxygen octahedra, containing disordered titanium vacancies, are separated by planes of cesium ions. Long-exposure precession photographs showed diffuse superlattice diffraction effects in the form of continuous streaks parallel to b_0^*. These have been analyzed in terms of models for two-dimensional ordering of the interlayer cesium ions. Annealing of melted samples below 700°C causes a transformation of the I-centered structure to a C-centered structure of the $K_x(M_yTi_{2-y})O_4$ type in which 3-D ordering of cesium occurs.

Introduction

New alkali metal titanates, with layer structures related to that of lepidocrocite, FeOOH (*1*), were first described by Reid et al. (*2*). They reported two series of compounds in which M^{3+} and M^{2+}, respectively, substitute for tetravalent titanium in puckered layers of edge- and corner-shared octahedra. In each case, charge balance is maintained by incorporation of interlayer alkali elements, giving the series $A_x[M_x^{3+}Ti_{2-x}]O_4$, A = Rb,Cs, and $Cs_x[M_{x/2}^{2+}Ti_{2-x/2}]O_4$, $0.6 < x < 0.8$. These compounds are of current interest because they display a variety of ion-exchange reactions with both aqueous and molten ion-exchange salts (*3*). Both series of compounds have I-centered orthorhombic cells with $a_0 \sim 3.8$ Å, $b_0 \sim 17$ Å, $c_0 \sim 3.0$ Å for the cesium salts.

Recently, Hervieu and Raveau (*4*) have described an extension of this structure type to a new series of nonstoichiometric cesium titanates, $Cs_x[\square_{x/4}Ti_{2-x/4}]O_4$, $\square$ = vacancy, $0.58 \leq x \leq 0.90$, prepared by reacting TiO_2 and $CsCO_3$ in air at temperatures in the range 300–700°C. From electron microscopy studies, Hervieu and Raveau showed that the majority of the crystals in their preparation had I-centered orthorhombic cells and were isostructural with $Cs_x(M,Ti)_2O_4$ (*2*). Whereas charge balance for the interlayer cesium in these latter compounds is maintained by substitution of M^{2+} and M^{3+} for tetravalent titanium, Hervieu and Raveau proposed that titanium vacancies in the octahedral layers gave charge balance in the new series. A phase showing a similar diffraction pattern has been previously reported as having the composition

0022-4596/87 $3.00

$Cs_{0.30}TiO_{2.15}$ (*5*). This was prepared by ion exchange of Cs^+ in hydrated TiO_2 followed by heating at 700°C. It can be reformulated as $(Cs_2O)_{0.3}Ti_2O_4$, suggesting an alternate structural model comprising TiO_2 layers alternating with layers of neutral Cs_2O. The same composition was recently reported for cesium titanate prepared by ion exchange of Cs^+ in melt-prepared $K_2Ti_2O_5$ crystals, followed by heating at 900°C (*6*).

We have recently reported the results of a phase study of the Cs_2O–TiO_2 system in the temperature range 850–1200°C (*7*). An I-centered orthorhombic phase isostructural with $Cs_x(M,Ti)_2O_4$ (*2*) was identified at a $TiO_2 : CsO_{0.5}$ molar ratio of 3 : 0 (referred to as the platelet phase because of its micaceous habit). Single crystals of the platelet phase, (*P*), were obtained from samples heated above 1115°C and cooled rapidly. Long-exposure precession photographs showed diffuse superlattice diffraction effects in the form of continuous streaks parallel to b^*, which were interpreted as due to ordering of interlayer cesium ions.

We report here the results of preparative studies on the platelet phase and of structure refinements using X-ray intensity data collected for two single crystals. We report also a semiquantitative analysis of the diffuse superlattice reflections in terms of models for the interlayer cesium ordering.

Preparative Studies

Experimental

The syntheses were carried out with Fisher-certified TiO_2 (anatase form) and reagent-grade $CsNO_3$ (BDH). Weighed mixtures corresponding to a range of molar ratios, $TiO_2/CsNO_3$ = 2.6 to 3.2, were intimately mixed and ground together, pelleted, and reacted in air at temperatures in the range 800–1120°C, for times varying from 0.5 to 20 hr. Reacted samples were usually ground, repelleted, and given a second heat treatment. The reaction products were cooled in a desiccator to avoid moisture uptake. Some samples were then exposed to air and the uptake of water recorded as a function of time. For some samples, the pellets were contained within platinum crucibles and the weight change monitored as a function of heating time to measure the volatilization rate of cesium. Single crystals were obtained from samples that were reacted at temperatures above 1115°C (for Ti/Cs < 3.0) or above 1100°C (Ti/Cs ≥ 3.0) for several hours then cooled rapidly.

The phases in the reaction products were identified from powder XRD patterns taken with a Philips diffractometer fitted with a graphite monochromator and employing Cu$K\alpha$ radiation.

Results and Discussion

The results of the synthesis experiments are summarized in Table I. Here we have retained the nomenclature of platelet (*P*) and needle (*N*) phase for phases with $TiO_2 : CsO_{0.5}$ molar ratios of 3.0 and 2.5, respectively (*7*). Actually, all products contained two platelet phases with slightly different layer separations as reflected in b_0 values of about 17.2 Å (*P*) and 17.0 Å (*P'*). The relative amounts of the two phases were dependent on the reaction temperature. At 800°C, the *P* phase predominated; at about 1000°C, *P* and *P'* were present in about equal amounts, while samples quenched from the melt contained only *P'*. The corresponding XRD powder patterns, in the region of the (060) reflection, are shown in Fig. 1.

At 800°C the platelet phase was the only product (except for minor unreacted TiO_2) of single equilibrations over the full range of compositions studied. However, when the samples were reground and reheated, the platelet phase was found to have a very

TABLE I

SYNTHESIS RESULTS FOR THE $CsO_{0.5}$–TiO_2 SYSTEM IN AIR

Temperature (°C)	Time (hr)	Heat	Molar ratio TiO_2:$CsNO_3$ in reaction mixture					
			2.6	2.8	2.9	3.0	3.1	3.2
800	20	1st	P[a] (trace A)	P (trace A)	P + minor A	P + minor A	P + minor A	
	20	2nd	P + N	P (trace N)	P (trace A)	P + minor A	P + minor A	
850	20	1st	P + N	P (trace A)		P + minor A		
	20	2nd	N + minor P	P + N		P + trace, N, A		
900	4	1st		P (trace R)	P (trace R)	P (trace R, A)	P (trace R, A)	
	4	2nd		P + N	P (trace N, R)	P (trace N, R)	P (trace R)	P + minor R
950	4	1st		P (trace N, R)		P (trace R)		P + minor R
	4	2nd		N + minor P		P + N		P + minor R
975	2	1st		P + minor N (trace R)		P (trace R)		P + minor R
	2	2nd		N + P + minor R		N + R (trace P)		P + minor R
1000	2	1st		P + N	P (trace R)	P (trace R)	P (trace R)	P + minor R
	2	2nd		N (trace P, R)	N (trace P, R)	P + N (trace R)	P (trace N, R)	P + minor R
1050	0.5	1st		P + minor N		P (trace R)		P + minor R
		2nd		N + trace R		N + P (trace R)		
1100	1	1st		N + trace R		N + minor R		N + minor R

[a] P = platelet phase, $Cs_x(Ti_{2-x/4}\square_{x/4})O_4$; N = needle phase, $Cs_2Ti_5O_{11}$ (7): A = anatase; R = rutile.

narrow composition range, centered at a TiO_2:$CsO_{0.5}$ ratio of about 2.9. Compositions with higher Cs contents contained the N phase whereas those with lower Cs contents contained excess TiO_2 (anatase form). The narrowness of the single-phase region is confirmed by the refined lattice parameters for the P phase in Table II, which show no consistent change with change in the Ti:Cs ratio of the reaction mixture, in contrast to the results of Hervieu and Raveau for samples prepared below 700°C (*4*).

Reaction products that were exposed to air gradually increased in weight due to uptake of water, up to a maximum of about 5 wt% after 2 days. This was accompanied by an increase in the layer separation, as measured by an increase in b_0 up to about 17.5 Å. For example, the refined parameters for a sample with TiO_2:$CsO_{0.5}$ = 3.0, reacted at 900°C, then left in air overnight, are a_0 = 3.816(2), b_0 = 17.54(2), c_0 = 2.962(2) Å. Thermogravimetric analysis run on the hydrated sample showed weight losses at 70 and ~200°C. An infrared spectrum showed broad bands at 3400 and 1620 cm^{-1}, corresponding to H-bonded water. The cell parameters reported by Hervieu and Raveau (*4*), for platelet phases prepared below 700°C, have b_0 values in the range 17.3–17.4 Å which probably correspond to partially hydrated compounds.

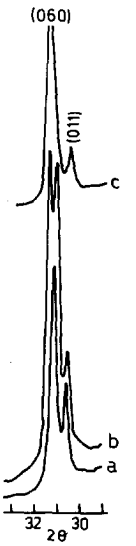

FIG. 1. Diffractometer trace in the region of the (060) reflection for preparations at (a) 800°C, (b) 1000°C, (c) 1120°C.

TABLE II

REFINED LATTICE PARAMETERS (Å) FOR THE P[a] PHASE FROM DIFFERENT SYNTHESES (TABLE I)

Reaction temperature (°C)		Molar ratio TiO_2 : $CsNO_3$ in reaction mixture				
		2.8	2.9	3.0	3.1	3.2
800	a_0	3.839(1)	3.835(1)	3.835(1)	3.831(1)	
1st heat	b_0	17.221(8)	17.222(9)	17.210(7)	17.263(6)	
	c_0	2.963(1)	2.965(1)	2.965(1)	2.961(1)	
800	a_0	3.828(1)	3.829(1)		3.833(1)	
2nd heat	b_0	17.237(6)	17.259(4)		17.247(4)	
	c_0	2.963(1)	2.964(1)		2.965(1)	
900	a_0	3.833(1)	3.830(1)	3.831(1)	3.830(1)	3.831(1)
1st heat	b_0	17.222(8)	17.247(5)	17.224(7)	17.234(5)	17.240(6)
	c_0	2.966(1)	2.962(1)	2.967(1)	2.965(1)	2.962(1)
900	a_0		3.831(1)	3.831(1)	3.831(1)	3.831(1)
2nd heat	b_0		17.247(5)	17.223(7)	17.236(5)	17.219(3)
	c_0		2.963(1)	2.964(1)	2.966(1)	2.964(1)
1050	a_0			3.832(1)		3.832(1)
1st heat	b_0			17.036(4)		17.050(7)
	c_0			2.965(1)		2.965(1)
1120	a_0	3.835(2)				3.833(1)
	b_0	17.02(1)				17.063(9)
	c_0	2.961(1)				2.961(1)

[a] All samples from syntheses experiments contained a mixture of two P phases with b_0 values of about 17.2 (P) and 17.0 (P'). The above parameters correspond to the *dominant* phase in each product.

With increasing temperature of preparation, the *P'* phase ($b_0 \simeq 17.0$ Å) gradually became the dominant phase as commented on above. This phase was metastable, and regrinding and reheating converted it to a mixture of the needle phase plus rutile, as previously reported (*7*) and shown in Table I. At 1100°C, just below the solidus, mixtures of needle phase and rutile formed, even on the first equilibration. However, samples heated above the solidus and cooled rapidly showed only *P'* over the full composition range studied (plus rutile due to Cs volatilization). A powder XRD pattern for a sample prepared at 800°C is shown in Fig. 2a. In addition to sharp reflections indexable by an I-centered orthorhombic cell, approximately 3.8 × 17 × 3 Å (*7*), the pattern shows a broad hump centered at $2\theta \simeq 25°$ (Cu$K\alpha$) which we interpret as due to short-range interlayer cesium ordering, cf. the streaks of diffuse intensity observed in single-crystal diffraction patterns for $Tl_x(Mg_{x/2}Ti_{2-x/2})O_4$ (*8*).

Transformation of I-Centered to C-Centered Structure

The XRD patterns of samples quenched from the melt changed markedly when the samples were annealed at low temperatures, as shown in Fig. 2b. The broad hump at $2\theta = 25°$ is replaced by sharp reflections at $2\theta \simeq 22.5$ and 27°, and the intensities of some of the I-centered cell reflections decrease dramatically, e.g., (121), (051) at $2\theta \simeq 40°$. A number of new reflections appear that can be indexed by a C-centered orthorhombic cell, analogous to that for $K_x(M_yTi_{2-y})O_4$ (*9*), e.g., (041), (061).

The ease of conversion from the I-cen-

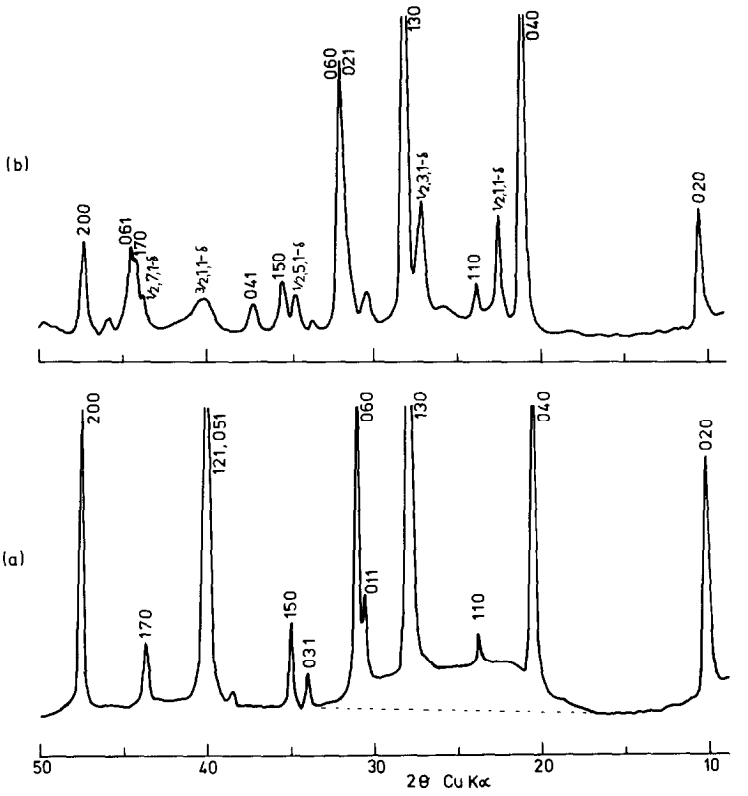

FIG. 2. X-Ray diffractograms for samples prepared at (a) 800°C, (b) melted at 1120°C, then annealed at 550°C.

tered to the C-centered structure was found to be dependent on the preliminary heat treatment. For samples that had first been melted and quenched, lines due to the C-centered structure appeared in the XRD patterns after annealing for only a day at 550°C, whereas samples preheated below the solidus showed only minor conversion even after a few weeks at 550°C. For the premelted samples, the formation of the C-centered phase was first discernible in the XRD patterns of samples annealed at 400°C, and the conversion rate was at a maximum at 550–600°C. Increasing the temperature of an annealed sample to 700°C brought about a transformation back to the I-centered phase and a loss of long-range cesium ordering, as evidenced by a return of the broad hump at $2\theta \simeq 25°$ in the XRD pattern.

A precession study of large single crystals grown from the melt and annealed at 550°C for several weeks showed no evidence of the transformation to the C-centered structure. The conversion reaction is apparently limited to microcrystalline material obtained by rapid quenching of melted compositions.

An indexing of the XRD pattern for the C-centered structure is shown in Fig. 2. Refined lattice parameters are $a_0 = 3.853(4)$, $b_0 = 16.88(2)$, $c_0 = 2.960(6)$ Å. The transformation involves a contraction in the separation between layers, reflected in a decrease of b_0 from 17.0 to 16.9 Å, and a slight expansion of the layers along a_0. The reflec-

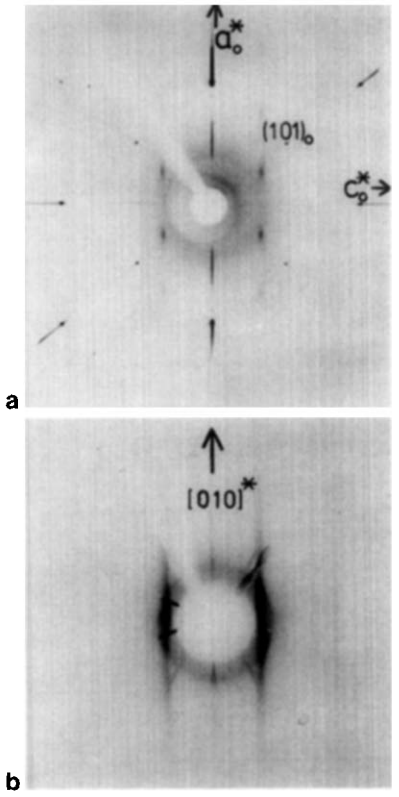

FIG. 3. Precession photographs for $Cs_x[Ti_{2-x/4}\square_{x/4}]O_4$. (a) [010] zone axis diffraction pattern. (b) Upper level [001] zone axis pattern, showing diffuse superlattice streaks parallel to b_0^*.

tions due to cesium ordering were indexed by analogy with reported superlattice reflection indexing in $Tl_x(Mg_{x/2}Ti_{2-x/2})O_4$ (*8*) and $Cs_xTi_{2-x/4}O_4$ (*9*). The indices are of the type $(h_0/2, k_0, l_0 \pm \delta)$, with h_0, k_0 odd, and $\delta = 0.39$, corresponding to a superlattice with $a = 2a_0$ and with c incommensurate with respect to c_0. Models for cesium ordering will be discussed in a later section.

Single-Crystal Studies

X-Ray diffraction studies, including structure refinements, were carried out on single crystals from two preparations. Crystal 1 derived from a reaction of a 2-molar ratio of TiO_2 and $CsNO_3$ at 1125°C, whereas crystal 2 was grown from a 3.2-molar ratio mixture at 1100°C. The latter reaction product contained the platelet phase and rutile, whereas the former contained the platelet phase together with a quenched liquid phase. The crystals from the two preparations have almost identical unit cell parameters and diffraction characteristics. In both cases, precession photographs display sharp reflections that can be indexed with an I-centered orthorhombic cell, $a_0 \simeq 3.83$, $b_0 \simeq 17.0$, $c_0 \simeq 2.96$ Å, together with diffuse diffraction effects in the form of ribbons of diffuse intensity parallel to b_0^*, as illustrated in Fig. 3b.

Intensity data sets for the sharp reflections were collected for both crystals and used to refine the average structure. The diffuse superlattice reflections were then analyzed to determine the local (two-dimensional) ordering of the cesium atoms.

Average Structure Refinement

The intensity data collections were carried out using a Siemens AED diffractometer. The conditions are summarized for the two crystals in Table III. Scattering factor curves for Cs, Ti, and O neutral atoms and anomalous dispersion coefficients were taken from International Tables for X-ray Crystallography, Vol. 4 (*10*). The calculations were performed using the SHELX 76 (*11*) system of programs. Refinement details are described for crystal 2.

The atomic coordinates for $Cs_{0.7}Mg_{0.35}Ti_{1.65}O_4$ (*2*) in *Imm*2 were used as starting parameters for the refinement. Refinement of coordinates and isotropic temperature factors converged at a high R-value of 0.23. The thermal parameter for cesium was high, $U = 0.054(3)$, and a difference Fourier map showed a large peak that corresponded to a second cesium atom in a centrosymmetric relation to Cs(1) (allowing for an origin shift). The intensity data were

TABLE III

SUMMARY OF DATA COLLECTION PARAMETERS

	Crystal 1	Crystal 2
Crystal dimensions (mm)	0.200 × 0.346 × 0.023	0.260 × 0.046 × 0.031
Unit cell parameters (Å)	a_0 = 3.829(3)	a_0 = 3.831(3)
	b_0 = 17.012(17)	b_0 = 17.021(18)
	c_0 = 2.962(3)	c_0 = 2.964(3)
Data collection parameters (common to both crystals)	Mo$K\alpha$ radiation	
	$\theta - 2\theta$ scan, 4–70°, 2θ	
	Scan rate 0.03° sec^{-1}	
	One standard reflection, measured every 3 hr, showed less than 2% intensity variation	
	962 measured reflections	
	h, 0 to 6; k, −27 to 27; l, −4 to 4	
Linear absorption coefficient	10.26 mm^{-1}	10.26 mm^{-1}
Max and min transmission factors	0.81, 0.13	0.73, 0.58
Number of unique reflections	281	281
R-value for equivalent reflections	0.009	0.026
Number of reflections used in refinement, $I > 3\sigma(I)$	238	230
Final R, R_w	0.084, 0.075	0.080, 0.087

reaveraged according to point symmetry *mmm* and a centrosymmetric model constructed in space group *Immm*. This involved a split cesium site, at ±(0, 0, 0.14), corresponding to a cesium–cesium separation of ~0.8 Å along c_0. Refinement of coordinates, anisotropic temperature factors, and cesium site occupancy proceeded smoothly and converged at R = 0.084 for 230 observed reflections with $I > 3\sigma(I)$. At this stage, the titanium site was fully occupied and the cesium site occupancy refined to 0.330(7), corresponding to a Ti/Cs ratio of 3.03.

Next, the titanium site occupancy was reduced to 0.92 to be consistent with the titanium-vacancy model, $Cs_x[Ti_{2-x/4}\square_x]O_4$, proposed by Hervieu and Raveau (*4*). Refinement of all parameters converged at R = 0.080, with a cesium site occupancy of 0.304(6), corresponding to Ti/Cs = 3.03. Finally, both cesium and titanium site occupancies were released and all parameters refined. Although a further reduction in R to 0.073 resulted, there were high correlations (0.8–0.85) between the scale and site occupancies. The refined site occupancies were 0.80(2) and 0.27(1) for titanium and cesium, respectively, giving a Ti/Cs ratio of 2.96. A difference Fourier map showed a peak near the origin, at (0, 0.02, 0), and peaks at (0, 0.32, 0), (0.5, 0.5, 0). The latter two peaks correspond to titanium and cesium sites displaced by $\frac{1}{2}c_0$ and are consistent with a minor component of the C-centered K-type structure (*9*) observed by Hervieu and Raveau (*4*). Some refinements were carried out in which these sites were partially occupied and the site occupancies refined. However, there was very little change to the R-factor and the refined site occupancies were very small (0.011(4), 0.017(6) for Cs and Ti, respectively).

The final atomic coordinates and temperature factors for both crystals are listed in Table IV. Observed and calculated structure factors may be obtained from the authors.

TABLE IV

FINAL POSITIONAL AND ANISOTROPIC THERMAL PARAMETERS (Å²)

Atom	Population parameter	x	y	z	U_{11}	U_{22}	U_{33}	U_{12}	U_{13}	U_{23}
Crystal 1										
Cs	0.302(5)	0	0	0.1363(16)	0.022(1)	0.028(1)	0.105(4)	0	0	0
Ti	0.92	0	0.3093(1)	½	0.0052(7)	0.0202(9)	0.0134(8)	0	0	0
O(1)		0	0.2196(3)	0	0.003(2)	0.018(2)	0.015(2)	0	0	0
O(2)		0	0.3765(3)	0	0.008(2)	0.012(2)	0.015(2)	0	0	0
Crystal 2										
Cs	0.304(6)	0	0	0.1439(20)	0.023(2)	0.039(2)	0.113(6)	0	0	0
Ti	0.92	0	0.3091(1)	½	0.0048(9)	0.030(1)	0.011(1)	0	0	0
O(1)		0	0.2193(5)	0	0.0001(24)	0.030(9)	0.011(3)	0	0	0
O(2)		0	0.3755(5)	0	0.011(3)	0.023(3)	0.011(3)	0	0	0

Description

The average structure is shown in projection down a_0 in Fig. 3 of Ref. (*7*). Relevant bond lengths and angles are given in Table V. This structure type has been described in detail by Reid *et al.* (*2*) and only some features will be elaborated on here.

The puckered octahedral sheets may be described either as cubic stacking of goethite-type (*12*) double-chains of edge-shared octahedra or as a fusion of pairs of duttonite-type ($VO(OH)_2$ (*13*)) planar sheets of edge- and corner-shared octahedra. These two alternative descriptions are emphasized in projection along c_0 and b_0, respectively, as shown in Figs. 4 and 5. The undulating surface of the octahedral sheets contains 2-coordinated anions, O(2), along the ridges and 4-coordinated anions, O(1), in the troughs. In lepidocrocite, FeOOH(1), the structure is built of such layers: the anion sites O(1) and O(2) are occupied by O^{2-} and OH^-, respectively, and Pauling's electroneutrality role is satisfied for both sites. However, in the TiO_2 layers of the *P* phase, both sites are occupied by oxygen. The formal valence sum is 2.67 and 1.33 for O(1) and O(2), respectively. The sites are thus severely over- and undersaturated, respectively, and this is reflected in long Ti–O(1) bonds, 2.12 Å, and short Ti–O(2) bonds, 1.86 Å. These distances result from a displacement of the titanium atoms by 0.2 Å from the octahedra centers toward the O(2)–O(2) edges.

TABLE V

SELECTED BOND LENGTHS (Å) AND ANGLES (°), CRYSTAL 2

Ti	–O(1)	(×2)	1.974(2)		
	–O(1)′	(×2)	2.128(6)		
	–O(2)	(×2)	1.864(5)		
O(1)	–O(1)′	(×4)	2.636(7)	O(1) –Ti–O(1)′	79.8(1)
	–O(2)	(×4)	2.909(7)	O(1) –Ti–O(2)	98.5(1)
O(1)′	–O(1)′		2.962	O(1)′–Ti–O(1)′	88.2(3)
	–O(2)	(×2)	2.657(12)	O(1)′–Ti–O(2)	83.2(3)
O(2)	–O(2)		2.962	O(2) –Ti–O(2)	105.3(4)
Cs	–O(2)	(×4)	3.044(6)	Cs–Cs	3.82(1)
Cs	–O(2)′	(×4)	3.433(6)	Cs–Cs′	3.923(3)
				Ti–Ti	2.962
				Ti–Ti′	3.147(2)

Very similar lattice parameters, atomic coordinates, and temperature factors were obtained for crystals 1 and 2 (Tables II and III) despite the fact that they were prepared from quite different reaction mixtures. This is consistent with the narrow homogeneity range established from the phase studies re-

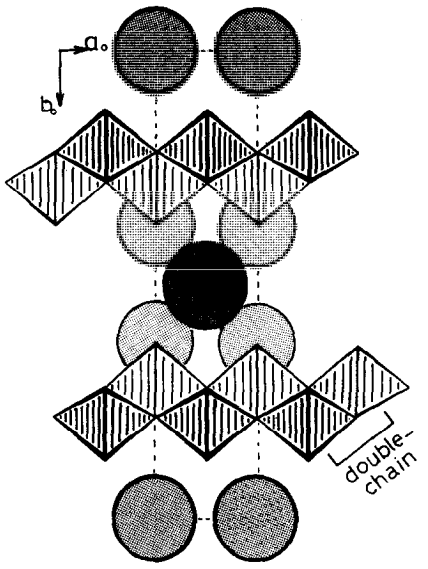

FIG. 4. Projection of the structure of $Cs_x[Ti_{2-x/4}\square_{x/4}]O_4$ along [001]. Double chains of edge-shared octahedra centered at $z = 0$ and $z = \frac{1}{2}$ (light and dark shading, respectively) link by edge-sharing to form stair-like (010) sheets. Large and small circles respresent cesium and oxygen, scaled to their ionic radii, to illustrate the packing of cesium in channels along c_0. Light and dark shaded cesium atoms at $z = \frac{1}{2}$, and $z = 0$, respectively.

ported above and contrasts with the results of Hervieu and Raveau (*4*), for the phase prepared below 700°C, where it has a wide range of homogeneity, $Cs_xTi_{2-x/4}O_4$, $0.58 < x < 0.90$.

Composition of the Platelet Phase

The composition of the platelet phase may be formulated either as $Cs_x(Ti_{2-x/4}\square_{x/4}]O_4$ (model 1) or as $(CsO_{0.5})_yTi_2O_4$ (model 2). The former model has been proposed by Hervieu and Raveau and contains interlayer Cs^+ ions, with charge balance maintained by titanium site vacancies. The latter case contains neutral interlayer Cs_2O molecules and the titanium sites in the octahedral layers are fully occupied. In principle, the question as to which of the two models is correct should be resolved from the structure refinement. Indeed, the improvement in the refinement on reducing the titanium site occupation parameter lends support to the first model. In practice, however, we find, in agreement with previous electron microscopy studies (*4*), that the crystals contain regions with different ordering of the cesium atoms due to local slipping of successive octahedral layers by $\frac{1}{2}c_0$. This produces elements of the C-centered structure adopted by $K_x(M_yTi_{2-y})O_4$ (*9*). This disorder of the interlayer cesium atoms makes it difficult to locate light interlayer atoms such as oxygen and puts some doubt on the validity of the occupation parameters obtained from the refinement.

An indirect test of the two models may be made by using the bond lengths obtained from the refinement to calculate valence sums using empirical bond length–bond strength parameters (*14*). This has been carried out for crystal 2, assuming an ordered sequence of cesium atoms and vacancies, or oxygen, as shown in Fig. 5, and a Ti/Cs ratio of 3 for both models. This corresponds to stoichiometries $Cs_{0.615}[Ti_{1.846}\square_{0.154}]O_4$ and $(CsO_{0.5})_{0.67}Ti_2O_4$ for models 1 and 2, respectively. For model 2, the interlayer oxygen, O(3), was placed at (0, 0.025, 0), consistent with the strongest peak observed in the difference Fourier map. The results are given in Table VI. For the atoms making up the octahedral layers, Ti,

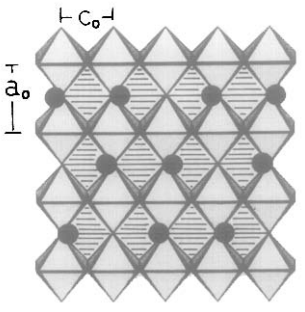

FIG. 5. Projection of the structure of $Cs_x[Ti_{2-x/4}\square_{x/4}]O_4$ along [010]. Ordering of interlayer cesium atoms corresponding to a $3c_0$ superstructure is shown.

TABLE VI

ELECTROSTATIC VALENCE SUMS

		Model 1 $Cs_{0.615}[Ti_{1.846}\square_{0.154}]O_4$		Model 2 $(CsO_{0.5})_{0.67}Ti_2O_4$
		d	s_i	s_i
Ti–O(1)	×2	1.974	1.259	1.259
–O(1)′	×2	2.128	0.852	0.852
–O(2)	×2	1.863	1.702	1.702
Σs_i			3.813 (3.69)[a]	3.813 (4.0)
Cs–O(1)	×2	3.755	0.087	0.087
–O(2)	×4	3.044	0.695	0.695
–O(2)′	×4	3.433	0.314	0.314
–O(3)[b]		2.571	—	0.530
–O(3)′		3.876	—	0.035
Σs_i			1.096 (1.0)	1.661 (1.0)
O(1)–Cs	×0.615	3.755	0.027	0.029
–Ti	2 × 923	1.974	1.163	1.260
–Ti′	2 × 923	2.128	0.787	0.853
Σs_i			1.977 (2.0)	2.142 (2.0)
O(2)–Cs	4 × 0.308	3.044	0.216	0.232
–Cs′	4 × 0.308	3.433	0.097	0.104
–Ti	2 × 0.923	1.863	1.565	1.702
Σs_i			1.878 (2.0)	2.038 (2.0)
O(3)–Cs	×2	2.571		1.059
–Cs′	×2	3.876		0.070
Σs_i				1.129 (2.0)

[a] Formal valences are given in parentheses.
[b] O(3) at (0, 0.025, 0).

O(1) and O(2), the agreement between Σs_i and the formal valences is equally satisfactory for both models. However, for the interlayer atoms, model 1 gives much closer agreement with the expected formal valences. For model 2, the calculated Σs_i at the Cs site is very high, 1.66, and Σs_i at the interlayer oxygen site O(3) is much too low, 1.13, suggesting that interlayer Cs_2O will be unstable relative to interlayer Cs^+ ions.

Interlayer Cesium Ordering

In addition to the sharp reflections used in the above refinements of the average structure, long-exposure precession photographs showed ribbons of diffuse intensity parallel to b_0^* as shown in Fig. 3b. These ribbons intersect the $a_0^*c_0^*$ reciprocal lattice section (r.l.s.) as short rods elongated parallel to a_0^*, Fig. 3a, with indices ($h_0/2$, $l_0 \pm$

δ), where h_0 is odd and δ is in the range 0.35–0.39 for different crystals. In the following discussion we will consider the case of δ = 0.33, corresponding to a commensurate superlattice spacing $c = 3c_0$.

A schematic representation of the $a_0^*c_0^*$ r.l.s. is given in Fig. 6. The superlattice reflections are confined to rows with odd half-integral multiples of a_0^*. The intensities of the diffuse streaks, when integrated over their length, have magnitudes that are comparable to those of the sharp, average-cell reflections, and that decrease slowly with increasing diffraction angle. We have interpreted these diffuse reflections as being diffracted intensity from short-range ordering of interlayer cesium atoms as previously proposed by Hervieu and Raveau (*4*). The continuous streak-line character of the superlattice reflections parallel to b_0^* indicates that there is little or no correlation between the cesium ordering in successive layers. Within a layer, the large cesiums are constrained to lie in channels parallel to c_0 as shown in projection in Fig. 4. The superlattice periodicity $c = 3 \times c_0$ is consistent with an ordering of (□–Cs–Cs–□–) chains in the channels. The structural model for ordering then reduces to a two-dimensional problem of stacking of these chains along a_0.

Structure factor calculations have been carried out for various chain stackings, shown on the left-hand side of Fig. 6(b–d). The corresponding $a_0^*c_0^*$ r.l.s. are shown next to the models in Fig. 6. The models incorporate the cesium displacements determined from the average structure refinement (for crystal 2). The diffraction data are plotted as circles with area proportional to F^2 (No Lp corrections applied) which allows a qualitative comparison with the experimental results. The two-dimensional models assume no correlation between the superlattice ordering in successive layers. However, the *average* structure in successive layers is related by body centering (Fig. 4) and we have taken this into account

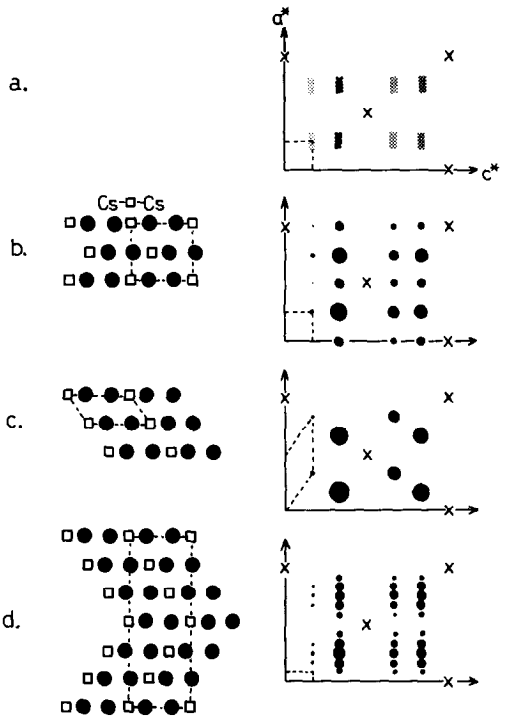

FIG. 6. (a) A schematic representation of the [010] zone axis diffraction pattern shown in Fig. 3a. (b)–(d) show different models for two-dimensional stacking of (Cs_2–□–) chains (LHS) and the corresponding calculated diffraction patterns (RHS) in which the areas of diffraction spots are proportional to F^2. Subcell reflections are shown by crosses.

in the calculated patterns by omitting the reflections with $h_0 + l_0 = 2n + 1$ (these would have a calculated intensity for a two-dimensional model).

As described above, to a first approximation, the superlattice reflections can be indexed by an orthogonal cell with $a = 2a_0$, $c = 3c_0$. However, it was not possible to construct a model in this simple superlattice that is compatible with the diffraction data. An example is shown in Fig. 6b. This type of model gives superlattice reflections along the rows (00*l*), (10*l*), (20*l*), etc., in contradiction to the observed diffraction pattern. Models which do *not* give reflections on these rows must meet the requirement that the superstructure, projected into the *aver-*

age cell along a, loses its superlattice periodicity along c. Examples of such models, with orthogonal cells with $a = 3a_0$ and $6a_0$, respectively, are shown in Figs. 6c and d. The latter model may be described as periodic twinning of model 6c, or of ordered intergrowth of models 6b and 6c. The corresponding diffraction pattern is very similar to the observed pattern, especially if allowance is made for small correlation lengths for the ordering. If the ordering is confined to small domains, the spots will be spread laterally and coalesce to form rods along a^* as experimentally observed.

The cesium ordering in relation to the octahedral layer is shown in Fig. 5. The cesium atoms are 10-coordinated, with two sets of four bonds to O(2) at 3.04 and 3.43 Å in a distorted cube arrangement and two longer bonds to O(1) at 3.75 Å. The Cs–Cs separation between adjacent cesium atoms along [001] is 3.79 Å. Such pairs are separated by 5.09 Å.

The simple commensurate models shown in Fig. 6 are easily modified to account for incommensurate periodicities corresponding to the observed range of $\delta = 0.35$–0.39, measured off precession photographs for crystals taken from a number of preparations. Since a δ value of 0.33 corresponds to a $3c_0$ ordering of the type (Cs–Cs–□–), and a δ value of 0.5 corresponds to a $2c_0$ ordering of alternate cesium atoms and vacancies (Cs–□–), then the observed range of δ may be accounted for by intergrowth of these two commensurate models. For example, a δ value of 0.375 corresponds to a 2:1 intergrowth (Cs–Cs–□–Cs–Cs–□–Cs–□–), with a Cs/Cs + □ occupancy factor of 0.625. Note that, in general, the cesium occupancy of the (010) layers is given by $(1 - \delta)$. If we formulate the composition according to Hervieu and Raveau's model, $Cs_x\square_{1-x}[Ti_{2-x/4}\square_{x/4}]O_4$, then, for the observed δ range of 0.35–0.39, the corresponding range of x is 0.65 to 0.61, and the resulting Ti/Cs ratio range using the above formula is 2.83 to 3.03. This gives a composition range centered at a Ti/Cs ratio of about 2.9, as experimentally observed in the phase equilibria studies (Table I). In the alternate formulation, as $(CsO_{0.5})_xTi_2O_4$, the observed range of δ corresponds to a Ti/Cs atomic ratio range of 3.08 to 3.28, which is inconsistent with the phase equilibria results.

The C-Centered Phase

As discussed in an earlier section, annealing melted samples at ~550°C causes a transformation from the I-centered structure to a C-centered structure of the $K_{0.8}Mg_{0.4}Ti_{2.6}O_4$ type (*9*). The transformation is achieved by a sliding of the octahedral layers relative to one another by $c_0/2$. The nearest-neighbor anion coordination of the larger interlayer cation changes from distorted cubic to trigonal prismatic. This type of coordination is unlikely for the very large Cs^+ ion and it presumably is displaced along c_0 relative to the position occupied by K^+ (*9*). The δ value for the C-centered structure is 0.39, corresponding to a composition $Cs_{0.61}Ti_{1.847}O_4$, Ti/Cs = 3.03. In contrast to the I-centered structures, the cesium-ordering reflections are sharp, indicating that the cesium ordering is correlated between layers as well as within layers. A related ordering of Ti atoms and vacancies must occur in the octahedral layers. In the $2a_0$ superlattice, the superlattice reflections have indices of the type $(h, k, l \pm \delta)$, h and k both odd, consistent with C-entering for the cesium atoms. Thus, in successive (010) layers, equivalent [001] chains of Cs and □ are related by $\frac{1}{2}a$. Long-term annealing experiments are in progress to prepare pure, well-ordered samples of the C-centered phase so that it can be characterized by a structure refinement.

References

1. F. J. Ewing, *J. Chem. Phys.* **3,** 420 (1935).
2. A. F. Reid, W. G. Mumme, and A. D. Wadsley, *Acta Crystallogr., Sect. B* **24,** 1228 (1968).

3. W. A. ENGLAND, J. E. BIRKETT, J. B. GOODENOUGH, AND P. J. WISEMAN, *J. Solid State Chem.* **49,** 300 (1983).
4. M. HERVIEU AND B. RAVEAU, *Rev. Chim. Minér.* **18,** 642 (1981).
5. S. A. ONORIN AND V. V. VOL'KHIN, *Zh. Prikl. Khim.* **49,** 27 (1976).
6. Y. FUJIKI, Y. KOMATSU, T. SASAKI, AND N. OHTA, *Nippon Kagaku Kaishi* **10,** 1656 (1981).
7. I. E. GREY, I. C. MADSEN, J. A. WATTS, L. A. BURSILL, AND J. KWIATKOWSKA, *J. Solid State Chem.* **58,** 350 (1985).
8. A. VERBAÈRE, M. DION, AND M. TOURNOUX, *Rev. Chim. Minér.* **12,** 156 (1975).
9. D. GROULT, C. MERCEY, AND B. RAVEAU, *J. Solid State Chem.* **32,** 289 (1980).
10. International Tables for X-Ray Crystallography, Vol. IV, Kynoch Press, Birmingham (1974).
11. G. M. SHELDRICK, *SHELX 76, in* "Program for Crystal Structure Determination," Universiy of Cambridge, England (1976).
12. W. HOPPE, *Z. Kristallogr.* **103,** 73 (1940).
13. H. T. EVANS, JR., AND M. E. MROSE, *Acta Crystallogr.* **11,** 56 (1958).
14. J. D. BROWN AND K. K. WU, *Acta Crystallogr. Sect. B* **32,** 1957 (1976).